ACS APPLIED NANO MATERIALS

Article

Cite This: ACS Appl. Nano Mater. 2019, 2, 418−428

www.acsanm.org

Visible-Light-Triggered Release of Sulfonamides in MOF/Ag-Based Nanoparticle Composites: Performance, Mechanism, and DFT Calculations

Xue-Yan Xu,[†] Jing Zhang,[‡] Xudong Zhao,[‡] Huifen Fu,[†] Chun Chu,[†] Peng Wang,[†] and Chong-Chen Wang*,[†]

[†]Beijing Key Laboratory of Functional Materials for Building Structure and Environment Remediation, Beijing Advanced Innovation Center for Future Urban Design, Beijing University of Civil Engineering and Architecture, Beijing 100044, P. R. China

[‡]College of Chemical and Biological Engineering, Taiyuan University of Science and Technology, Taiyuan 030012, P. R. China

Supporting Information

ABSTRACT: Visible-light-responsive materials sparked wide interest due to visible light possessing some merits like no byproduct formation, environmental friendliness, and nearly zero energy consumption. In this work, UiO-66-NH_2/Ag_2CO_3 (UAC-X) composites with outstanding adsorption and visible-light-triggered desorption performance toward sulfonamides (SAs) like sulfamethoxazole (SMX), sulfisoxazole (SIX), and sulfamethazine (SMT) were reported. It was believed that the interactions between $-NH_2$ from SAs and Ag^+ of Ag_2CO_3 (UAC-X) nanoparticles contributed to the outstanding adsorption performance toward the SAs. The conversion from Ag^+ to Ag^0 of the photosensitive Ag_2CO_3 (NPs) in the UAC-X composites led to the controlled delivery of SAs, in which the release performance could be tuned by the UiO-66-NH_2 proportion in UAC-X. Additionally, the DFT calculation results demonstrated that the binding energy of Ag^+-NH_2 (BE = −0.925 eV) is lower than the band gap of Ag_2CO_3 (BE = 2.3 eV), implying that the conversion from Ag^+ to Ag^0 contributed to the SAs desorption. The light-induced desorption will provide new strategies to realize environment friendly and inexpensive regeneration of adsorbents.

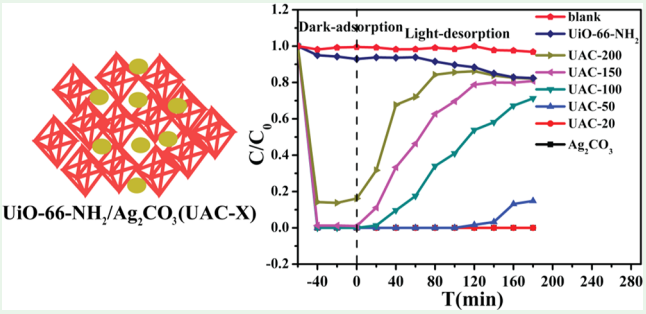

KEYWORDS: *visible-light-triggered, desorption, UiO-66-NH_2, sulfonamides, mechanism*

1. INTRODUCTION

The pharmaceutical and personal care products (abbreviated as PPCPs) are emerging as pseudo persistent organic pollutants,[1] including substances for the purpose of personal health/cosmetic reasons, along with the products to improve the livestock's growth and health.[2] Elevated levels of PPCPs have been detected in the aquatic and soil environment throughout the world, which exert serious threats to the ecological environment and even human health.[3−7] The antibacterial sulfonamides (SAs) are widely selected to prevent infectious diseases and to boost livestock growth, which resulted in their wide distribution in the environment annually.[8,9] The presence of SAs in the environment can become toxic to aquatic life and to humans via drinking water[10−12] and even increase drug resistance toward disease-causing bacteria.[13,14] Therefore, it is essential to monitor and remove the environmental PPCPs even at trace levels.

Several removal methods including adsorption,[15−18] advanced oxidation processes (AOPs),[19−21] and biological technologies[22,23] have been utilized to remove PPCPs from the aquatic systems. Adsorption has been shown to remove PPCPs from the environment due to their flexible and simple design, low initial cost, high efficiency, and easy operation.[24,25] Considering that conventional adsorption is generally a spontaneous process, chemical treatment (using organic solvents, acid or alkali) or energy is needed to achieve desorption, which might result in secondary pollution and massive energy consumption. Functional materials, which can be structurally switchable by light,[26−33] have attracted wide interest, since light, especially concentrated sunlight, possessed several advantages such as no byproducts, environmental friendliness, and nearly zero energy input.[34] Hence, visible-light-triggered desorption is highly preferred in the wide research fields ranging from environmental chemistry, materials science, and biology.[34−38]

In this paper, a series of UiO-66-NH_2/Ag_2CO_3 composites (UAC-X, X = 20, 50, 100, 150, and 200 mg of UiO-66-NH_2) were fabricated via an in situ ion-exchange solution method, which adopted $AgNO_3$, Na_2CO_3, and UiO-66-NH_2 as precursors. It was found that the suitable combination of

Received: November 3, 2018
Accepted: December 26, 2018
Published: December 26, 2018

Scheme 1. Fabrication of UiO-66-NH_2/Ag_2CO_3 Composites (UAC-X)

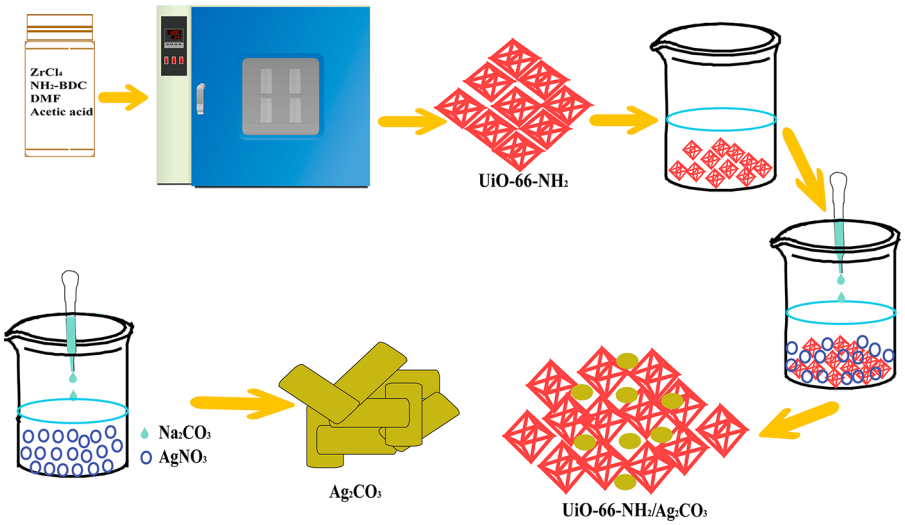

Ag_2CO_3 with UiO-66-NH_2 could achieve better adsorption performance than individual component and could accomplish visible-light-triggered controlled release. The adsorption−desorption activities of sulfamethoxazole (SMX), sulfisoxazole (SIX), and sulfamethazine (SMT) were determined, and the corresponding mechanism of light triggered desorption was proposed and clarified.

2. EXPERIMENTAL SECTION

2.1. Materials and Instruments. The details of materials and instruments were listed in the Supporting Information.

2.2. Fabrication of UiO-66-NH_2/Ag_2CO_3 Composites. UiO-66-NH_2 octahedra were synthesized following a reported solvothermal route with a minor modification.[39,40] Briefly, $ZrCl_4$ (1.05 g, 4.5 mmol) and 2-aminoterephthalic acid (NH_2−BDC 0.81g, 4.5 mmol) were dissolved in 40.0 mL of *N*,*N*-dimethylformamide (DMF). Then, acetic acid (17.0 mL) was mixed with the above solution to regulate the morphology of the products in a 100 mL Teflon-lined bomb. The Teflon-lined bomb was then heated in an oven at 293 K for 24 h. After cooling to room temperature, the products were collected by centrifugation and washed with ultrapure water for several times. The harvested light-yellow material was dried in an air oven at 333 K for 12 h.

UAC-X (X = 20, 50, 100, 150, and 200) composites were fabricated using a modified in situ ion-exchange solution method,[40−43] as illustrated in Scheme 1. Series UiO-66-NH_2/Ag_2CO_3 with UiO-66-NH_2/$AgNO_3$ weight ratio of 0.02/0.1 (UAC-20), 0.05/0.1 (UAC-50), 0.1/0.1 (UAC-100), 0.15/0.1 (UAC-150), and 0.2/0.1 (UAC-200) were prepared by using UiO-66-NH_2, $AgNO_3$, and Na_2CO_3 as precursors. Theoretically, series UiO-66-NH_2/Ag_2CO_3 composites were fabricated with the same weight of Ag_2CO_3 and the different weight of UiO-66-NH_2. For instance, the weight ratios of UiO-66-NH_2 and Ag_2CO_3 in UAC-100 and UAC-150 were calculated as 100/81 and 150/81, respectively. After filtration, the product was washed with ultrapure water several times, followed by being dried in an air oven at 333 K. For comparison, the pristine Ag_2CO_3 was synthesized from the same procedure as that for UAC-X composites except for the addition of UiO-66-NH_2.

2.3. Adsorption and Visible-Light-Triggered Desorption Experiment. Series batch experiments were conducted to evaluate the adsorption−desorption performance of UAC-X toward sulfonamides (SAs) including sulfamethoxazole (SMX), sulfisoxazole (SIX), and sulfamethazine (SMT). The adsorption activities of UAC-X toward SAs were tested by adopting 40.0 mL of SAs aqueous solution with concentration of 50.0 mg L^{-1} and 10.0 mg UAC-X particles at room temperature in a 50 mL quartz reactor. As well, 10.0 mg L^{-1} and 200.0 mg L^{-1} SMX aqueous solutions were also selected to explore the effect of concentration of target on desorption activity. After stirring for 60 min to achieve adsorption−desorption equilibrium in the dark, the light-triggered desorption was tested under visible light illumination (λ > 420 nm, Figure S1 in Supporting Information) from a 350 mW LED light source (PCX50A, Beijing Perfect Light Technology Co., Ltd.).

2.4. Theoretical Calculation. Density functional theory (DFT) with the Perdew−Burke−Ernzerh generalized gradient approximation calculations were conducted using DMol3 package, and double-numeric quality basis set with polarization functions was used for all the atoms.[44,45] A 0.005 hartree thermal smearing and a 0.37 nm real-space cutoff were adopted. The geometry convergence tolerances were 0.000 01 hartree, 0.02 hartree nm^{-1}, and 0.0005 nm for energy change, max force, and max displacement, respectively. During geometry optimization, all atoms were permitted to relax freely. The binding energy (BE) is defined as BE = $E_{tot} - E_{Ag_2CO_3} - E_{SMX}$, where E_{tot}, $E_{Ag_2CO_3}$, E_{SMX} are the energies of the Ag_2CO_3 with an adsorbed SMX molecule, the Ag_2CO_3, and the SMX molecule, respectively. The negative binding energy implies that the SMX molecules will be energetically favorable to be bonded with the Ag^+ in Ag_2CO_3.

3. RESULTS AND DISCUSSION

3.1. Characterizations of UAC-X Composites. The morphologies and structures of the UAC-X were characterized by TEM and PXRD. The TEM images (Figure 1 and Figure S2) demonstrated that Ag_2CO_3 nanoparticles were dispersed on the UiO-66-NH_2 substrates. UiO-66-NH_2 octahedrons as a deposition platform/substrate could affect the growth of Ag_2CO_3 crystals and minimize the aggregation of Ag_2CO_3 NPs. In detail, the higher UiO-66-NH_2 proportion in the UAC-X composites induced the smaller of Ag_2CO_3 nanoparticles. It was found that the particle size of Ag_2CO_3 decreased from 500 to 800 nm in the pure Ag_2CO_3 (Figure 1a) to 50−110 nm in UAC-150 (Figure 1c) and 50−60 nm in UAC-200 (Figure S2). The PXRD diffraction patterns (Figure 2a) of UiO-66-NH_2 match well with those reported.[39,46,47] For the pristine Ag_2CO_3 NPs, all of the diffraction peaks can be readily indexed to monoclinic phase (JCPDS card no. 00-026-0339 (RDB)).[48] The peaks of both UiO-66-NH_2 and Ag_2CO_3 can be clearly identified in PXRD patterns of UAC-X composites (Figure 2a). The different preferred orientation of UAC-X composites and the interaction between the incorporated Ag_2CO_3 and the UiO-66-NH_2 substrate resulted

DOI: 10.1021/acsanm.8b01979
ACS Appl. Nano Mater. 2019, 2, 418−428

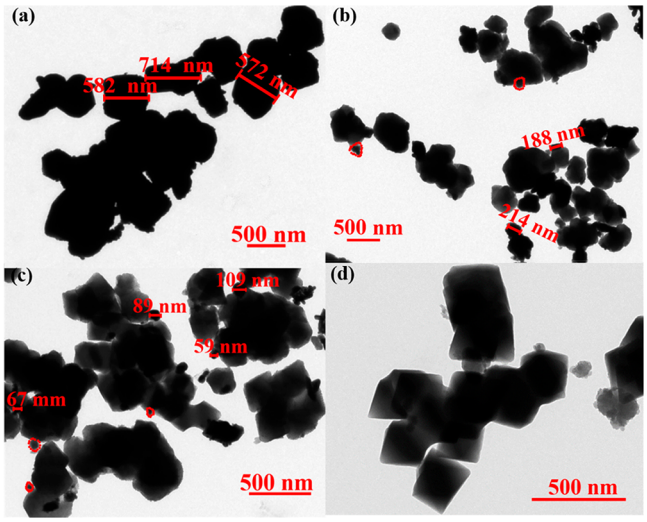

Figure 1. TEM images of (a) Ag_2CO_3, (b) UAC-100, (c) UAC-150, (d) UiO-66-NH_2.

in PXRD peaks of UAC-X near 20° that could not match well with Ag_2CO_3 or UiO-66-NH_2 individually. The slightly broader Ag_2CO_3 peak at ∼33° in UAC-X composites (including UAC-20, UAC-50, etc.) compared with that of pure Ag_2CO_3 indicates the smaller Ag_2CO_3 particle sizes in UAC-X composites, which is in agreement with the TEM images (Figure 1 and Figure S2). Clear fringe spacing of approximately 0.264 and 0.230 nm corresponding to the (130) and (031) crystal planes of Ag_2CO_3 ((JCPDS card no. 00-026-0339 (RDB) can be observed through the HRTEM image (Figure 3a), implying that Ag_2CO_3 NPs are successfully incorporated into UiO-66-NH_2.[49,50]

The successful deposition of Ag_2CO_3 nanoparticles on UiO-66-NH_2 substrate was further proved via FTIR spectra, as illustrated in Figure 2b. The two peaks at 664 and 769 cm^{-1} are attributed to Zr−O_2 clusters.[51] The peaks at 1449, 1382, 884, and 707 cm^{-1} were the characteristic peaks for CO_3^{2-} from Ag_2CO_3.[39] With UiO-66-NH_2 proportion growth, the peaks of Ag_2CO_3 at 1449, 1382, 884, and 707 cm^{-1} decreased gradually and the intensity of two sharp peaks (664 and 769 cm^{-1}) of Zr−O_2 cluster increased significantly.The XPS spectra in Figure 2c displayed the presence of Ag, C, O, Zr, and N elements in UAC-X, indicating the successful fabrication of both UiO-66-NH_2 and Ag_2CO_3. Additionally, the XPS results show that the Ag 3d peaks exhibited a slight shift to the higher binding energy in UAC-X compared to those of individual Ag_2CO_3, which might be assigned to the synergistic effect between the incorporated Ag_2CO_3 and the UiO-66-NH_2 substrate, further enhancing the light sensitivity of the final composite.[41] The TGA of individual UiO-66-NH_2 (Figure 2d) revealed that the weight losses from 200 to 450 °C were presumably due to the decomposition of the NH_2−BDC ligand, leaving the zirconium oxide derived from the "node" of UiO-66-NH_2 as residue.[52−54] It was worthy to note that there is over 20% weight loss before 300 °C, resulting from UiO-66-NH_2 not being activated before preparation of UAC-X. Considering the pore size of UiO-66-NH_2 (less than 1.0 nm, Figure S3) and the particle size of Ag_2CO_3 (500−800 nm), the solvent molecules in their pores and cages could not hinder the Ag_2CO_3 NPs formation inside UiO-66-NH_2. The pristine Ag_2CO_3 was decomposed thermally to Ag element via two

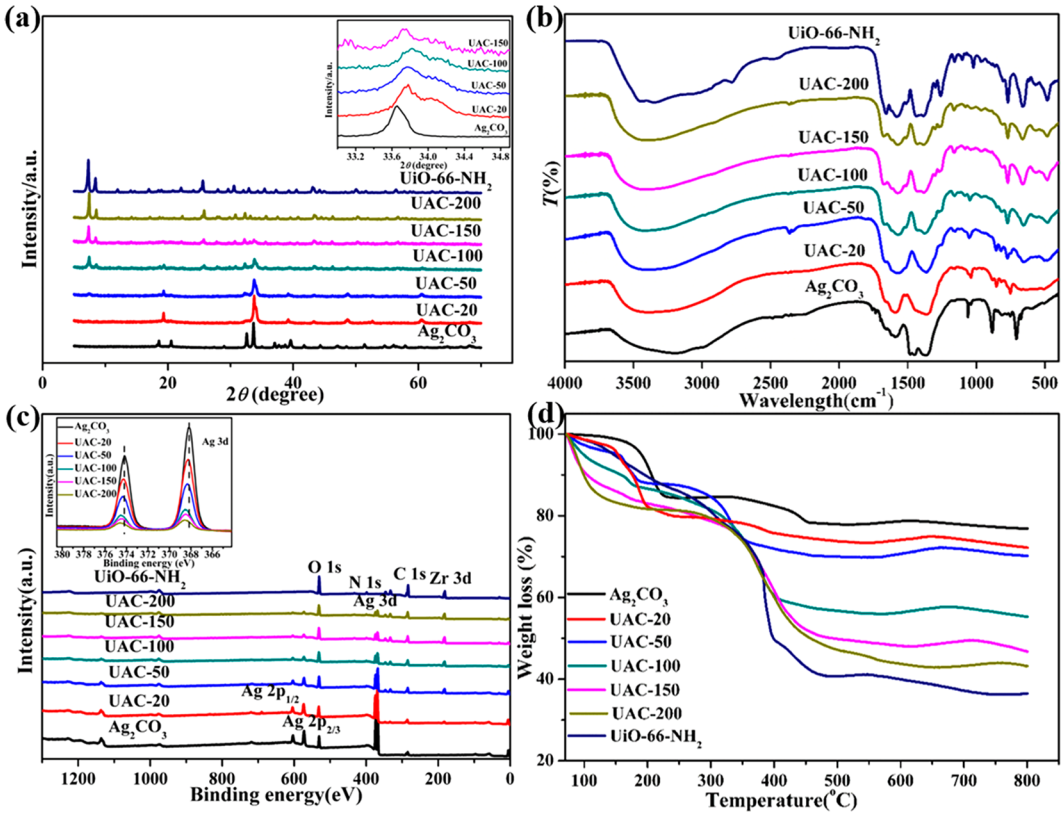

Figure 2. (a) PXRD patterns, (b) FTIR and (c) XPS spectra, and (d) TGA curves of Ag_2CO_3, UAC-X (X = 20, 50, 100, 150, and 200 mg) composites, and UiO-66-NH_2.

DOI: 10.1021/acsanm.8b01979
ACS Appl. Nano Mater. 2019, 2, 418−428

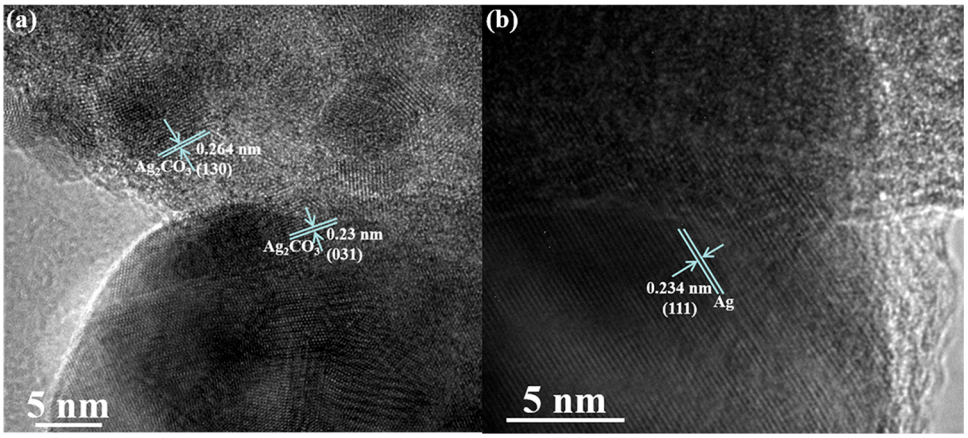

Figure 3. HRTEM images of UAC-150 of (a) as-prepared and (b) after adsorbing SMX in dark and under visible light illumination for 3 h.

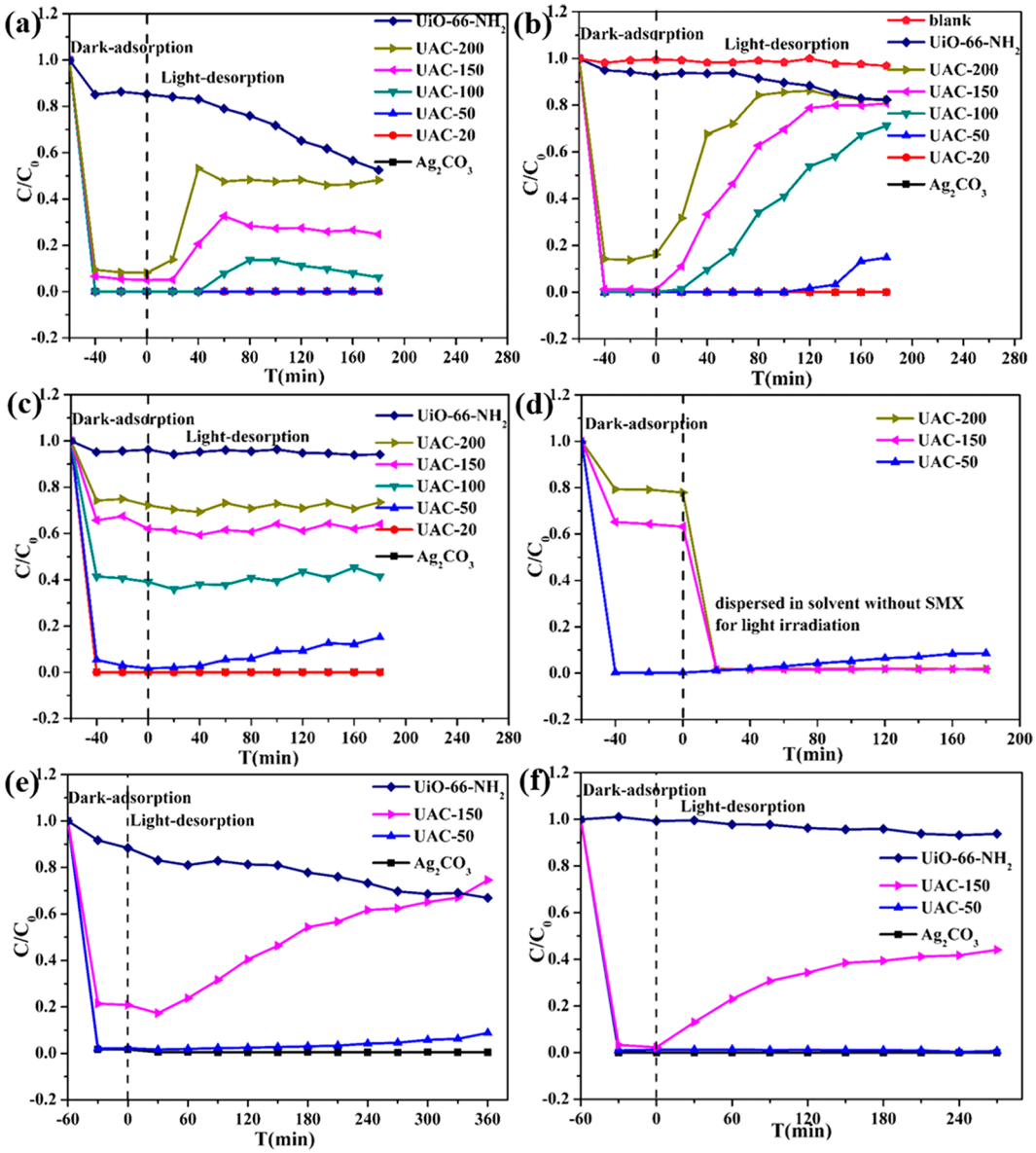

Figure 4. Uptake and relaese activity of Ag_2CO_3, UAC-X (X = 20, 50, 100, 150, and 200 mg) composites, and UiO-66-NH_2 toward SMX with different initial concentrations, (a) 10 mg L^{-1}, (b) 50 mg L^{-1}, (c) 200 mg L^{-1}, (d) 200 mg L^{-1} (adsorption in dark), in aqueous solution without SMX (desorption under visible light illumination). Uptake and release activity of Ag_2CO_3, UAC-X (X= 20, 50, 100, 150, and 200 mg) composites, and UiO-66-NH_2 toward (e) SIX and (f) SMT with initial concentration of 50 mg L^{-1}.

DOI: 10.1021/acsanm.8b01979
ACS Appl. Nano Mater. 2019, 2, 418−428

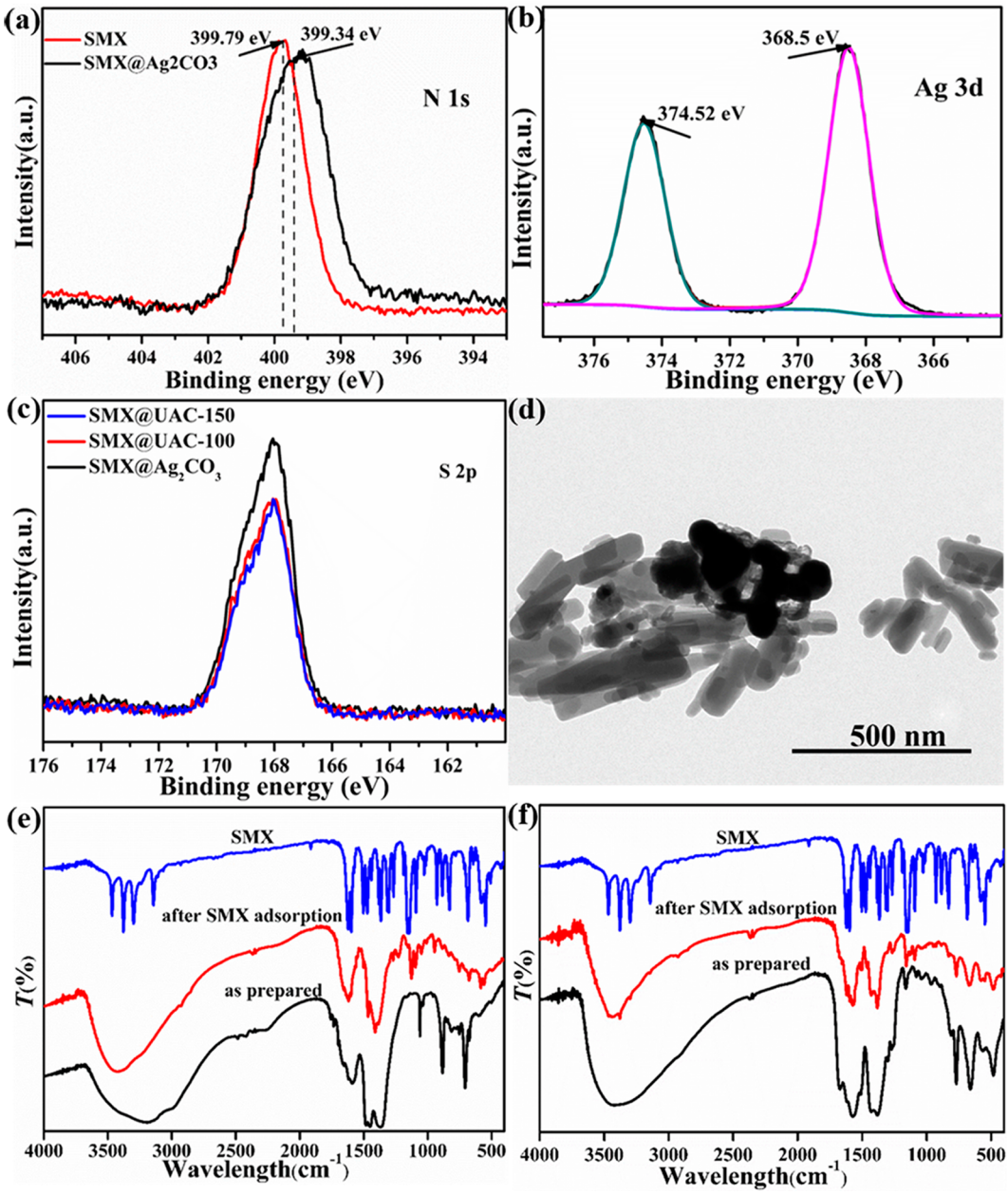

Figure 5. (a) N 1s and (b) Ag 3d XPS spectra of SMX and Ag_2CO_3 after SMX adsorption in the dark. (c) S 2p XPS spectra in Ag_2CO_3, UAC-100, and UAC-150 after SMX adsorption in the dark. (d) TEM images of UAC-100 after SMX adsorption in the dark. (e) FTIR spectra of as-synthesized Ag_2CO_3, SMX, Ag_2CO_3 after SMX adsorption in the dark. (f) FTIR spectra of as-synthesized UAC-150, SMX, UAC-150 after SMX adsorption in the dark.

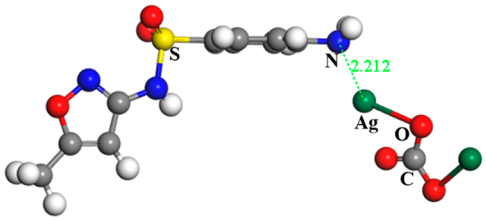

Figure 6. Optimal configurations obtained via DFT calculations of NH_2−Ag^+ coordination interaction.

distinct steps with Ag_2O as the intermediate compound.[42] The weight losses of UAC-X composites matched well with UiO-66-NH_2 and Ag_2CO_3, and the residues were the mixtures of zirconium oxides[52−54] and metallic Ag.[42] The standard N_2 adsorption−desorption measurements (Table S1 in Supporting Information) confirmed that the Ag_2CO_3 NPs were anchored with UiO-66-NH_2, in which the BET surface area decreased from 745.92 m^2 g^{-1} (UiO-66-NH_2) to 26.029 m^2 g^{-1} (UAC-20).

3.2. Adsorption and Visible-Light-Triggered Desorption Performance of UAC-X toward SAs. *3.2.1. Adsorption toward SAs of UAC-X. 3.2.1.1. Adsorption Performance.* It was found that UAC-X exhibited higher adsorption performances toward SAs than UiO-66-NH_2. Under dark condition, Ag_2CO_3 particles could adsorb nearly 100% selected SAs with initial concentration of 50 mg L^{-1} for SIX and SMT and 200 mg L^{-1} for SMX within 20 min, whereas the individual UiO-66-NH_2 could only capture less than 20% of the selected SAs with initial concentration of 50 mg/L, as illustrated in parts c,

DOI: 10.1021/acsanm.8b01979
ACS Appl. Nano Mater. 2019, 2, 418−428

Scheme 2. Proposed Mechanism of the Visible-Light Controlled Desorption of SAs from UAC-X Composites

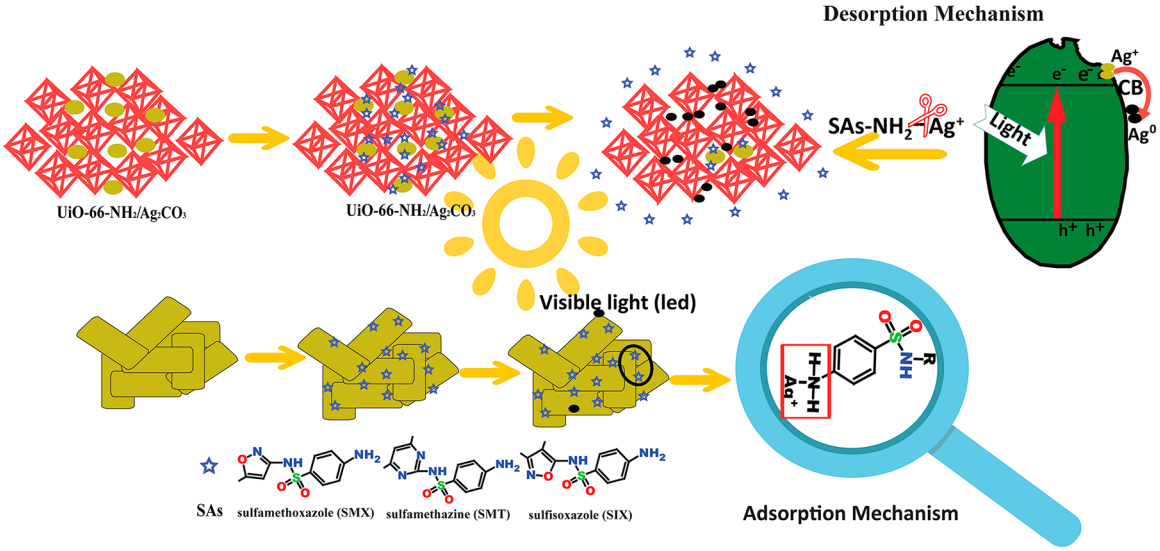

e, and f of Figure 4. Moreover, Ag_2CO_3, UAC-20, and UAC-50 can achieve nearly 100% SMX uptake (with initial concentration of 200 mg L^{-1}) within 20 min in the dark, while UAC-100, UAC-150, and UAC-200 only captured approximately 61.0%, 37.9%, and 27.8% SMX after 1 h under the identical conditions. It was implied that the adsorption activities of UAC-X were mainly controlled by Ag_2CO_3 NPs. Therefore, the increase of UiO-66-NH_2 proportion induced decreased adsorption performance, in which the adsorption amounts decreased from 1902 (Ag_2CO_3) to 1578.7 (UAC-20), 921.0 (UAC-50), 509.4 (UAC-100), 314.0 (UAC-150), and 245.5 mg g^{-1} (UAC-200).

3.2.1.2. Adsorption Mechanism. It is believed that the interactions between Ag^+ and $-NH_2$ of SAs were conducive to the outstanding adsorption activity of Ag_2CO_3 for SAs.[55,56] Specifically, the XPS results show an obvious red shift of XPS spectra from 399.79 to 399.34 eV for N 1s in NH_2 attached to SMX after adsorption process on Ag_2CO_3 (Figure 5a). On the contrary, the Ag 3d peaks demonstrate a blue shift from 368.17 eV ($3d_{5/2}$) and 374.19 eV ($3d_{3/2}$) in prepared Ag_2CO_3 (Figure S4)[57,58] to 368.5 and 374.52 eV in SMX@Ag_2CO_3 (Figure 5b), affirming that the $-NH_2$ of SMX had a coordination effect with Ag^+ from Ag_2CO_3.[55] The Ag 3d and N 1s XPS spectra of UAC-100 and UAC-150 before and after SMX adsorption were shown in Figure S5 and Figure S6, which were in good agreement with the results of SMX@Ag_2CO_3. The difference of BE shift of Ag 3d and N 1s in SMX@Ag_2CO_3 and SMX@UAC-X could be attributed to the coordination between Ag^+ and $-NH_2$ tending to promote electrostatic attractions of Ag^+ ions resulting in the blue shift of Ag 3d, while the Ag^+-NH_2 coordination interaction tends to weaken the electrostatic attractions from $-NH_2$ group. Theoretically, 1.0 mol of Ag_2CO_3 is stoichiometrically interacted with 2.0 mol of SMX, implying that 1.0 g of Ag_2CO_3 can capture 1837 mg of SMX. Practically, the experimental adsorption capacity (1902 mg g^{-1}) of Ag_2CO_3 toward SMX was slightly higher than the calculated one (1837 mg g^{-1}), which might be ascribed to other interactions like electrostatic interaction, hydrogen bonding interaction, and so on.[59−64] As well, the poorest adsorption activity toward SAs of UiO-66-NH_2 revealed that SAs particle could not be adsorbed by pores of UiO-66-NH_2.

It can be seen from the TEM images (Figure 5d and Figure S7) that strip-like SMX was absorbed on the Ag_2CO_3, UAC-100, and UAC-150. Moreover, the S 2p peak originating from SMX in the XPS spectra (Figure 5c) could be observed, which affirmed that Ag_2CO_3, UAC-100, and UAC-150 have good adsorption activity toward SMX. In addition, the occurrence of several characteristic peaks of SMX at 3378.22, 3299.1, 3314, and 547.13 cm^{-1} was found in the FTIR spectra of SMX@Ag_2CO_3 and SMX@UAC-150, which further confirmed that SMX was adsorbed onto Ag_2CO_3 and UAC-150 (Figure 5e and Figure 5f).

Compared to as-prepared Ag_2CO_3, the new weight losses in TGA curves (Figure S8) of the Ag_2CO_3 treated with SMX adsorption in dark and under visible light illumination for 3 h matched well with the weight loss of SMX, in which the extra weight loss nearly was equal to the experimentally adsorbed SMX. As a result, Ag_2CO_3 could not achieve desorption and photocatalytic degradation for SMX upon visible light illumination. It was suggested that the coordination between Ag^+ in Ag_2CO_3 and $-NH_2$ in SMX in the dark could prevent the Ag_2CO_3 NPs' photocatalytic degradation behaviors.

3.2.2. Visible-Light-Triggered Release of SAs from UAC-X.

3.2.2.1. Release Performance. Among various stimuli, light is certainly prospective with the advantage of a high level of control over time and location.[65] The combination of UiO-66-NH_2 and Ag_2CO_3 (UAC-100/150/200) can achieve efficient uptake of several selected SAs and also accomplish good desorption toward these SAs under the visible light illumination. For example, the UAC-150 exhibited excellent desorption activity with maximum adsorption amount of 314 mg g^{-1}, and ∼80.8% adsorbed SMX was released upon visible light illumination (Figure 4b). In addition, 66.7% SIX and 43.7% SMT could be released by UAC-150, as illustrated in Figure 4e and Figure 4f. It is obvious that the desorption performance could be tuned by the UiO-66-NH_2 content in UAC-X composites. UAC-X with low content of UiO-66-NH_2 such as UAC-20 has good adsorption activity and poor desorption activity toward SMX, whereas larger content of UiO-66-NH_2 such as UAC-200 leads to decreased adsorption

DOI: 10.1021/acsanm.8b01979
ACS Appl. Nano Mater. 2019, 2, 418−428

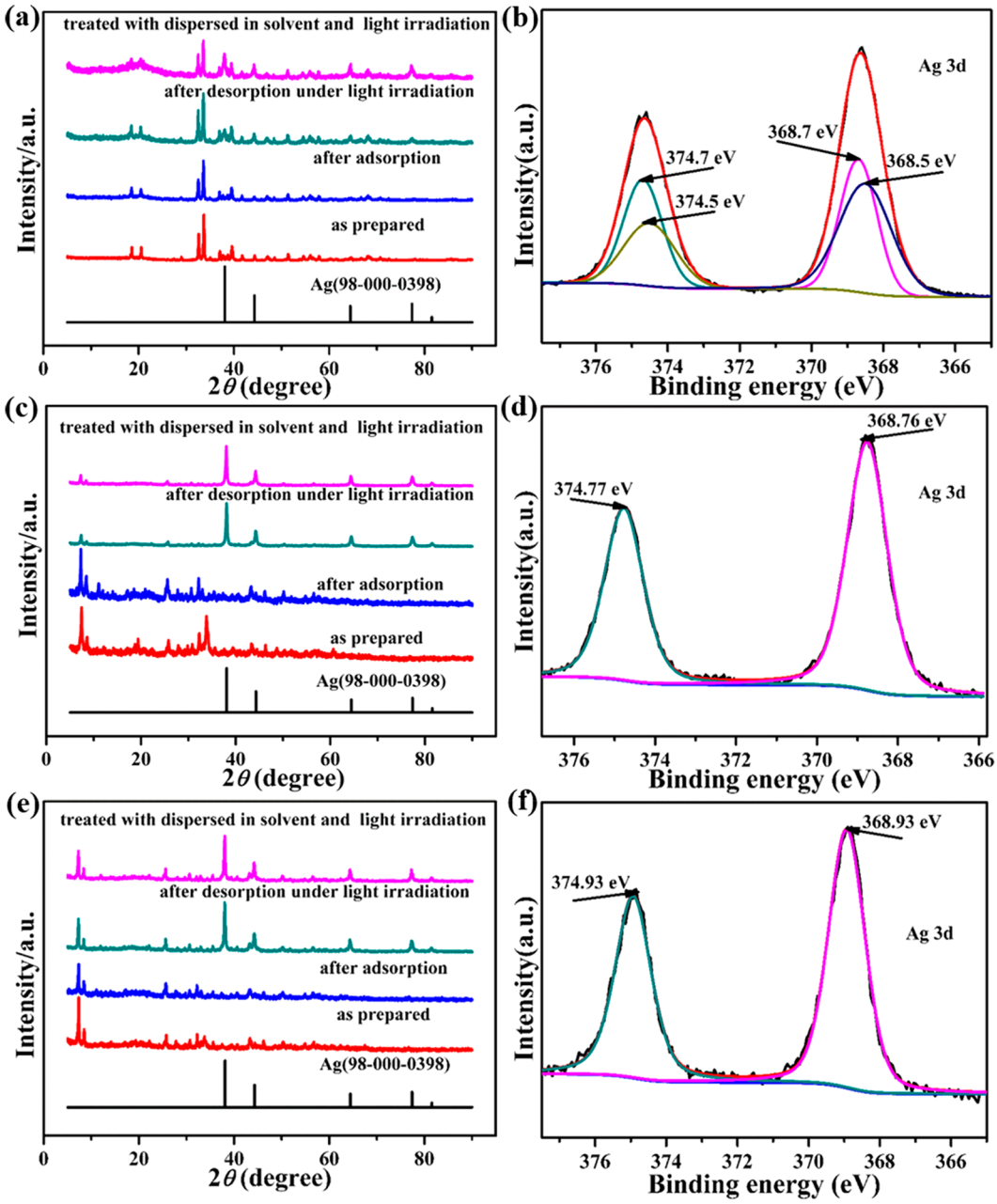

Figure 7. PXRD patterns of (a) Ag_2CO_3, (c) UAC-100, and (e) UAC-150 as-prepared, after SMX adsorption in the dark and visible-light-triggered desorption, treated with dispersion in aqueous solution without SMX and visible light irradiation for 3 h. Ag 3d XPS spectra of (b) Ag_2CO_3, (d) UAC-100, and (f) UAC-150 after adsorbing SMX in the dark and visible-light-triggered desorption.

and good visible-light-triggered desorption performance. In detail, the desorption performance of UAC-X for SMX with adsorption amount being 200 mg g^{-1} follows the order of 0% (UAC-20), 14.8% (UAC-50), 71.3% (UAC-100), and 80.8% (UAC-150), while under the identical condition, the adsorption capacity of UAC-200 toward SMX is 168 mg g^{-1}, and 83.5% SMX was released upon the visible light illumination. Furthermore, the desorption rate was positive related with the UiO-66-NH_2 proportion in UAC-X composites.

3.2.2.2. Effect of Concentration of SMX on Release Activity. At relative low initial concentration (10 and 50 mg L^{-1}), UAC-150 can achieve good uptake in the dark and visible-light-triggered release performance toward SMX, as depicted in Figure 4a and Figure 4b. However, at high initial concentration of SMX like 200 mg L^{-1}, no significant desorption can be detected with the presence of visible light (Figure 4c). It was believed that it was difficult to accomplish SMX desorption under visible light illumination using saturated UAC-X. This further affirmed that UAC-100 and UAC-150 saturated by SMX exhibited no visible-light-triggered desorption behaviors even in aqueous solution, as illustrated in Figure 4d. Additionally, the desorption activity of UAC-X toward SMX with lower initial concentration (10 mg L^{-1}) was lower than that SMX with relative higher initial concentration (50 mg L^{-1}). As a result, the UAC-X which has reached saturated adsorption could not release the SMX under visible light illumination. Furthermore, the release performance of UAC-X composites toward SMX was positive related to the experimental adsorption weight under their maximum/

DOI: 10.1021/acsanm.8b01979
ACS Appl. Nano Mater. 2019, 2, 418−428

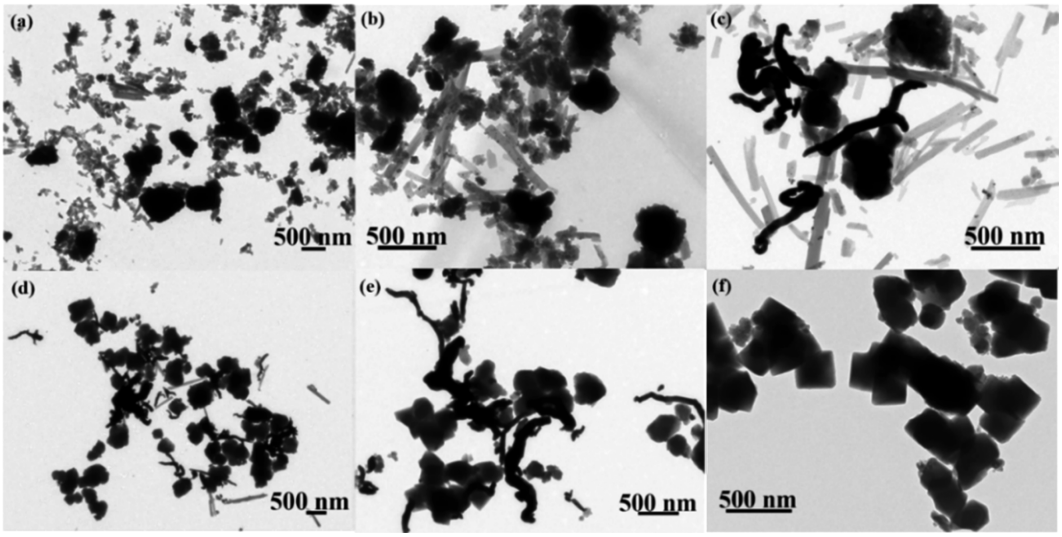

Figure 8. TEM images of (a) Ag_2CO_3, (b) UAC-20, (c) UAC-50, (d) UAC-100, (e) UAC-150, (f) UiO-66-NH_2 after SMX adsorption in the dark and then visible-light-triggered desorption.

saturated adsorption capacities. It was assumed that the Ag_2CO_3 NPs saturated by SMX with initial concentration of 200 mg L^{-1} in UAC-100 and UAC-150 composites had been wrapped with SMX, resulting in Ag_2CO_3 NPs that could not harvest light for the conversion from Ag^+ to Ag^0.

3.2.2.3. Visible Light Controlled Release Mechanism. It has been reported that Ag-containing compounds such as Ag_3PO_4, Ag_3VO_4, Ag_2CrO_4, and Ag_2CO_3 have outstanding photosensitive activity, in which the Ag^+ could be reduced to Ag^0 by obtaining e^- following eq 1 under light irradiation.[43,66] After adsorption, the optimal configuration between SMX and Ag_2CO_3 was shown in Figure 6 via DFT calculations. The coordination interaction of NH_2-Ag^+ was formed, which consisted of the proposed adsorption mechanism. The DFT calculation results displayed that the adsorption behavior of SMX could be attributed to chemical adsorption (BE = −0.925 eV). As well, the band gap energy of Ag_2CO_3 semiconductor was estimated to be 2.3 eV.[43] It could be concluded that the light with wavelength less than 539 nm can accomplish enough energy to produce photoinduced electrons to reduce Ag^+ to Ag^0. As a result, the conversion from Ag^+ to Ag^0 led to the SAs desorption, which could be further enhanced via increase of the UiO-66-NH_2 proportion in UAC-X composites. The Ag^+ in Ag_2CO_3 NPs of UAC-X composites can capture the photoinduced electrons to form Ag^0, followed by the breakdown of Ag^+-NH_2 interaction between Ag_2CO_3 and SAs (as illustrated in Scheme 2), which was proposed as the possible mechanism of visible light controlled SAs release from UAC-X. The smaller size Ag_2CO_3 NPs enhance the light harvesting,[67] which facilitated the efficiency and rate of conversion from Ag^+ to Ag^0, leading to adsorptive sites' (Ag^+) sharp reduction and subsequent desorption of SMX under visible light illumination. TEM results illustrated in Figure 1 and Figure S2 revealed that the smaller size Ag_2CO_3 NPs could be achieved via increase of the UiO-66-NH_2 proportion in the composites. Therefore, the desorption activities of UAC-X toward SMX increases with the UiO-66-NH_2 content.

$$Ag^+ + e^- \rightarrow Ag^0 \quad (1)$$

Judged by PXRD, XPS, and TEM analysis results, the enhanced reduction activity of Ag^+ can be obtained from smaller Ag_2CO_3 NPs in UAC-X. Obvious characteristic peaks belonging to Ag^0 in UAC-100/150 could be detected in Figure 7c, Figure 7e, and Figure S9, whereas for Ag_2CO_3/UAC-20, it is difficult to differentiate the Ag^0 due to the minor content via PXRD patterns after 3 h visible light irradiation. For Ag 3d of pristine Ag_2CO_3 treated with SMX adsorption in the dark and visible light triggered release, it exhibited both Ag^+ coordinated with $-NH_2$ in SMX (374.52 and 368.5 eV) and Ag^0 peaks (374.7 and 368.7 eV) (Figure 7b),[50] while there were only Ag^0 peaks (368.76 and 374.77 eV) in treated UAC-100/150, as illustrated in Figure 7d and Figure 7f. Additionally, due to the synergistic effect between the incorporated Ag_2CO_3 and the UiO-66-NH_2 substrate which is in agreement with the Ad 3d peakes shift in Figure 2c, the binding energy of Ag^0 in treated UAC-100/150 was higher than that of Ag_2CO_3. The TEM images displayed that the Ag^0 clusters increased with the increasing UiO-66-NH_2 proportion in UAC-X composites treated with SMX adsorption in the dark and visible-light-triggered release (Figure 8). HRTEM image (Figure 3b) could give further evidence of the presence of Ag^0 after SMX desorption upon the visible light illumination, in which the fringe spacing of 0.234 nm can be ascribed to the (111) crystal plane of Ag^0.[68] Furthermore, the residual SMX in the SMX@UAC-X composites decreased with increasing UiO-66-NH_2 proportion in UAC-X composites after visible light irradiation for 3 h. The results were in agreement with the PXRD and XPS results as stated above. As a result, the SMX desorption activity depended on the conversion efficiency from Ag^+ to Ag^0 which could be tuned by the UiO-66-NH_2 proportion in UAC-X composites. The desorption activity of UAC-50 with initial SMX concentration of 200 mg L^{-1} was inferior to that of 50 mg L^{-1}, which could be attributed to the high SMX content in the UAC-50 leading to low reduction efficiency from Ag^+ to Ag^0. Furthermore, the conversion from Ag^+ to Ag^0 was not ascribed to the presence of SMX, which was affirmed by the PXRD patterns of Ag_2CO_3, UAC-100, and UAC-150 being dispersed in aqueous solution without SMX and irradiated under visible light for 3 h (parts a, c, and e of Figure 7). It can be seen from the PXRD patterns that there were no Ag^0 peaks

DOI: 10.1021/acsanm.8b01979
ACS Appl. Nano Mater. 2019, 2, 418−428

presented in Ag_2CO_3 and UAC-X after adsorbing SMX in the dark. Hence, it could be concluded that the transformation from Ag^+ to Ag^0 under visible light irradiation might be the possible mechanism, as illustrated in Scheme 2. UiO-66-NH_2 could provide a platform to accomplish the distribution of Ag_2CO_3 NPs and subsequently tune the size of Ag_2CO_3 NPs to promote the SMX release.

4. CONCLUSION

In summary, UiO-66-NH_2/Ag_2CO_3 composites (UAC-X) were fabricated by incorporating UiO-66-NH_2 with Ag_2CO_3 via a facile in situ ion-exchange precipitation method in aqueous solution. The good distribution of fine Ag_2CO_3 NPs on the UiO-66-NH_2 substrate contributed to the good adsorption behavior and visible-light-triggered desorption activities of the UAC-X toward SMX, SIX, and SMT. Specifically, UAC-150 possesses high-performance adsorption activity (experimental adsorption amount: 200 mg g^{-1} for SMX, SIX, and SMT, respectively) and desorption activity toward SAs (release ratio being 80.8% for SMX, 66.7% for SIX, and 43.7% for SMT). Visible-light-induced conversion from Ag^+ to Ag^0 is considered to be the possible mechanism for the SAs visible-light-triggered release, which was confirmed by the density functional theory (DFT) calculation. Compared to our previous work on the visible-light-triggered release of SMX on UAP-X (UiO-66-NH_2/Ag_3PO_4) composites, in this work, three sulfonamides were selected as targets to test the light-triggered desorption performance of UAC-X (UiO-66-NH_2/Ag_2CO_3) composites. It was highlighted that the effect of concentration of SMX on release activity was investigated and the mechanism was further clarified via DFT calculation besides corresponding characterizations. This work further confirmed it is feasible to achieve visible-light-triggered desorption adopting the strategy of the combination between light sensitive Ag-based NPs and UiO-66-NH_2 MOFs substrate. As well, these composites might provide new possibility to develop unprecedented light-desorption-based sample pretreatment for GC and LC, which is potentially superior to the conventional thermal adsorption and solvoadsorption.

■ ASSOCIATED CONTENT

Supporting Information

The Supporting Information is available free of charge on the ACS Publications website at DOI: 10.1021/acsanm.8b01979.

Materials and instruments in detail, the wavelength distribution of PCX50A, TEM images of UAC-20 and UAC-150, the corresponding surface area of UiO-66-NH_2, the pore size distribution of UiO-66-NH_2, the XPS spectra for Ag 3d in Ag_2CO_3, Ag 3d and N 1s XPS spectra of UAC-100 and UAC-150 before and after SMX adsorption in dark, TEM images of Ag_2CO_3 and UAC-150 after SMX adsorption in dark, TGA curves of SMX@Ag_2CO_3 before and after visible light radiation for 3 h, a brief discussion on the water stability of UAC-X, PXRD patterns of UAC-X treated after adsorption SMX in dark and visible-light-triggered desorption (PDF)

■ AUTHOR INFORMATION

Corresponding Author

*E-mail: wangchongchen@bucea.edu.cn. Phone: +86 10 61209186. Fax: +86 10 61209186..

ORCID

Chong-Chen Wang: 0000-0001-6033-7076

Notes

The authors declare no competing financial interest.

■ ACKNOWLEDGMENTS

This work was supported by NSFC (Grants 51878023, 51578034), Beijing Talent Project (Grant 2018A35), Great Wall Scholars Training Program Project of Beijing Municipality Universities (Grant CIT&TCD20180323), Project of Construction of Innovation Teams and Teacher Career Development for Universities and Colleges Under Beijing Municipality (Grant IDHT20170508).

■ REFERENCES

(1) Wang, J.; Wang, S. Removal of Pharmaceuticals and Personal Care Products (PPCPs) from Wastewater: A Review. *J. Environ. Manage.* **2016**, *182*, 620−640.

(2) Daughton, C. G.; Ternes, T. A. Pharmaceuticals and Personal Care Products in the Environment: Agents of Subtle Change. *Environ. Health Perspect.* **1999**, *107*, 907−938.

(3) Kümmerer, K. Antibiotics in the Aquatic Environment - A Review. *Chemosphere* **2009**, *75*, 417−434.

(4) Nam, S.-W.; Jung, C.; Li, H.; Yu, M.; Flora, J. R. V.; Boateng, L. K.; Her, N.; Zoh, K.-D.; Yoon, Y. Adsorption Characteristics of Diclofenac and Sulfamethoxazole to Graphene Oxide in Aqueous Solution. *Chemosphere* **2015**, *136*, 20−26.

(5) Done, H. Y.; Halden, R. U. Reconnaissance of 47 Antibiotics and Associated Microbial Risks in Seafood Sold in the United States. *J. Hazard. Mater.* **2015**, *282*, 10−17.

(6) Zhang, Q.; Jia, A.; Wan, Y.; Liu, H.; Wang, K.; Peng, H.; Dong, Z.; Hu, J. Occurrences of Three Classes of Antibiotics in a Natural River Basin: Association with Antibiotic-Resistant Escherichia Coli. *Environ. Sci. Technol.* **2014**, *48*, 14317−14325.

(7) Le-Minh, N.; Khan, S. J.; Drewes, J. E.; Stuetz, R. M. Fate of Antibiotics during Municipal Water Recycling Treatment Processes. *Water Res.* **2010**, *44*, 4295−4323.

(8) Liu, F.-F.; Zhao, J.; Wang, S.; Xing, B. Adsorption of Sulfonamides on Reduced Graphene Oxides as Affected by pH and Dissolved Organic Matter. *Environ. Pollut.* **2016**, *210*, 85−93.

(9) Wang, F.; Ma, S.; Si, Y.; Dong, L.; Wang, X.; Yao, J.; Chen, H.; Yi, Z.; Yao, W.; Xing, B. Interaction Mechanisms of Antibiotic Sulfamethoxazole with Warious Graphene-Based Materials and Multiwall Carbon Nanotubes and the Effect of Humic Acid in Water. *Carbon* **2017**, *114*, 671−678.

(10) Lin, C.-Y.; Huang, S.-D. Application of Liquid-Liquid-Liquid Microextraction and High-Performance Liquid-Chromatography for the Determination of Sulfonamides in Water. *Anal. Chim. Acta* **2008**, *612*, 37−43.

(11) Wang, Z.; Li, Y.; Liang, X.; Zhang, S.; Shi, W.; Shen, J. Forcing Immunoassay for Sulfonamides to Higher Sensitivity and Broader Detection Spectrum by Site Heterologous Hapten Inducing Affinity Improvement. *Anal. Methods* **2013**, *5*, 6990−7000.

(12) Bao, Y.; Lim, T.-T.; Wang, R.; Webster, R. D.; Hu, X. Urea-Assisted One-Step Synthesis of Cobalt Ferrite Impregnated Ceramic Membrane for Sulfamethoxazole Degradation via Peroxymonosulfate Activation. *Chem. Eng. J.* **2018**, *343*, 737−747.

(13) Baquero, F.; Martínez, J.-L.; Cantón, R. Antibiotics and Antibiotic Resistance in Water Environments. *Curr. Opin. Biotechnol.* **2008**, *19*, 260−265.

(14) He, Z.; Cheng, X.; Kyzas, G. Z.; Fu, J. Pharmaceuticals Pollution of Aquaculture and its Management in China. *J. Mol. Liq.* **2016**, *223*, 781−789.

(15) Babel, S.; Kurniawan, T. A. Low-Cost Adsorbents for Heavy Metals Uptake from Contaminated Water: a Review. *J. Hazard. Mater.* **2003**, *97*, 219−243.

(16) Hou, S.; Wu, Y.-n.; Feng, L.; Chen, W.; Wang, Y.; Morlay, C.; Li, F. Green Synthesis and Evaluation of an Iron-Based Metal-Organic Framework MIL-88B for Efficient Decontamination of Arsenate from Water. *Dalton Trans* **2018**, *47*, 2222−2231.
(17) Wang, X.; Wang, X.; Wei, Z.; Zhang, S. Potent Removal of Cyanobacteria with Controlled Release of Toxic Secondary Metabolites by a Titanium Xerogel Coagulant. *Water Res.* **2018**, *128*, 341−349.
(18) Zhao, X.; Wang, K.; Gao, Z.; Gao, H.; Xie, Z.; Du, X.; Huang, H. Reversing the Dye Adsorption and Separation Performance of Metal-Organic Frameworks via Introduction of -SO_3H Groups. *Ind. Eng. Chem. Res.* **2017**, *56*, 4496−4501.
(19) Esplugas, S.; Bila, D. M.; Krause, L. G. T.; Dezotti, M. Ozonation and Advanced Oxidation Technologies to Remove Endocrine Disrupting Chemicals (EDCs) and Pharmaceuticals and Personal Care Products (PPCPs) in Water Effluents. *J. Hazard. Mater.* **2007**, *149*, 631−642.
(20) Herney-Ramirez, J.; Vicente, M. A.; Madeira, L. M. Heterogeneous Photo-Fenton Oxidation with Pillared Clay-Based Catalysts for Wastewater Treatment: A Review. *Appl. Catal., B* **2010**, *98*, 10−26.
(21) Wang, G.; Zhao, D.; Kou, F.; Ouyang, Q.; Chen, J.; Fang, Z. Removal of Norfloxacin by Surface Fenton System ($MnFe_2O_4$/H_2O_2): Kinetics, Mechanism and Degradation Pathway. *Chem. Eng. J.* **2018**, *351*, 747−755.
(22) Joss, A.; Zabczynski, S.; Göbel, A.; Hoffmann, B.; Löffler, D.; McArdell, C. S.; Ternes, T. A.; Thomsen, A.; Siegrist, H. Biological Degradation of Pharmaceuticals in Municipal Wastewater Treatment: Proposing a Classification Scheme. *Water Res.* **2006**, *40*, 1686−1696.
(23) Vasiliadou, I. A.; Molina, R.; Martínez, F.; Melero, J. A. Biological Removal of Pharmaceutical and Personal Care Products by a Mixed Microbial Culture: Sorption, Desorption and Biodegradation. *Biochem. Eng. J.* **2013**, *81*, 108−119.
(24) Jiang, J.-Q.; Ashekuzzaman, S. M. Development of Novel Inorganic Adsorbent for Water Treatment. *Curr. Opin. Chem. Eng.* **2012**, *1*, 191−199.
(25) Zhuang, Z.; Chen, H.; Lin, Z.; Dang, Z. Mn_2O_3 Hollow Spheres Synthesized Based on an Ion-Exchange Strategy from Amorphous Calcium Carbonate for Highly Efficient Trace-Level Uranyl Extraction. *Environ. Sci.: Nano* **2016**, *3*, 1254−1258.
(26) Boyer, J.-C.; Carling, C.-J.; Gates, B. D.; Branda, N. R. Two-Way Photoswitching Using One Type of Near-Infrared Light, Upconverting Nanoparticles, and Changing only the Light Intensity. *J. Am. Chem. Soc.* **2010**, *132*, 15766−15772.
(27) Yagai, S.; Kitamura, A. Recent Advances in Photoresponsive Supramolecular Self-Assemblies. *Chem. Soc. Rev.* **2008**, *37*, 1520−1529.
(28) Ferris, D. P.; Zhao, Y.-L.; Khashab, N. M.; Khatib, H. A.; Stoddart, J. F.; Zink, J. I. Light-Operated Mechanized Nanoparticles. *J. Am. Chem. Soc.* **2009**, *131*, 1686−1688.
(29) Zhu, Q.-L.; Sheng, T.-L.; Fu, R.-B.; Hu, S.-M.; Chen, L.; Shen, C.-J.; Ma, X.; Wu, X.-T. Redox-Responsive Photochromism and Fluorescence Modulation of Two 3D Metal-Organic Hybrids Derived from a Triamine-Based Polycarboxylate Ligand. *Chem. - Eur. J.* **2011**, *17*, 3358−3362.
(30) Sortino, S. Photoactivated Nanomaterials for Biomedical Release Applications. *J. Mater. Chem.* **2012**, *22*, 301−318.
(31) Wei, Y.; Han, S.; Kim, J.; Soh, S.; Grzybowski, B. A. Photoswitchable Catalysis Mediated by Dynamic Aggregation of Nanoparticles. *J. Am. Chem. Soc.* **2010**, *132*, 11018−11020.
(32) Shiraishi, Y.; Tanaka, K.; Shirakawa, E.; Sugano, Y.; Ichikawa, S.; Tanaka, S.; Hirai, T. Light-Ariggered Self-Assembly of Gold Nanoparticles based on Photoisomerization of Spirothiopyran. *Angew. Chem., Int. Ed.* **2013**, *52*, 8304−8308.
(33) Zhang, F.-M.; Dong, H.; Zhang, X.; Sun, X.-J.; Liu, M.; Yang, D.-D.; Liu, X.; Wei, J.-Z. Postsynthetic Modification of ZIF-90 for Potential Targeted Codelivery of Two Anticancer Drugs. *ACS Appl. Mater. Interfaces* **2017**, *9*, 27332−27337.
(34) Zhang, S.; Peng, Y.; Jiang, W.; Liu, X.; Song, X.; Pan, B.; Yu, H.-Q. Light-Triggered Reversible Sorption of Azo Dyes on Titanium Xerogels with Photo-Switchable Acetylacetonato Anchors. *Chem. Commun.* **2014**, *50*, 1086−1088.
(35) Beharry, A. A.; Woolley, G. A. Azobenzene Photoswitches for Biomolecules. *Chem. Soc. Rev.* **2011**, *40*, 4422−4437.
(36) Lin, Q.; Bao, C.; Cheng, S.; Yang, Y.; Ji, W.; Zhu, L. Target-Activated Coumarin Phototriggers Specifically Switch on Fluorescence and Photocleavage upon Bonding to Thiol-Bearing Protein. *J. Am. Chem. Soc.* **2012**, *134*, 5052−5055.
(37) Wu, B.; Yin, R.; Zhang, G.; Yu, C.; Zhang, S. Effects of Water Chemistry on Decolorization in Three Photochemical Processes: Pro and cons of the UV/AA process. *Water Res.* **2016**, *105*, 568−574.
(38) Zhang, F.-M.; Sheng, J.-L.; Yang, Z.-D.; Sun, X.-J.; Tang, H.-L.; Lu, M.; Dong, H.; Shen, F.-C.; Liu, J.; Lan, Y.-Q. Rational Design of MOF/COF Hybrid Materials for Photocatalytic H_2 Evolution in the Presence of Sacrificial Electron Donors. *Angew. Chem.* **2018**, *130*, 12282−12286.
(39) Wang, R.; Gu, L.; Zhou, J.; Liu, X.; Teng, F.; Li, C.; Shen, Y.; Yuan, Y. Quasi-Polymeric Metal−Organic Framework UiO-66/g-C_3N_4 Heterojunctions for Enhanced Photocatalytic Hydrogen Evolution under Visible Light Irradiation. *Adv. Mater. Interfaces* **2015**, *2*, 1500037.
(40) Xu, X.-Y.; Chu, C.; Fu, H.; Du, X.-D.; Wang, P.; Zheng, W.; Wang, C.-C. Light-Responsive UiO-66-NH_2/Ag_3PO_4 MOF-Nanoparticle Composites for the Capture and Release of Sulfamethoxazole. *Chem. Eng. J.* **2018**, *350*, 436−444.
(41) Sha, Z.; Chan, H. S.; Wu, J. Ag_2CO_3/UiO-66(Zr) Composite with Enhanced Visible-Light Promoted Photocatalytic Activity for Dye Degradation. *J. Hazard. Mater.* **2015**, *299*, 132−140.
(42) Yu, C.; Li, G.; Kumar, S.; Yang, K.; Jin, R. Phase Transformation Synthesis of Novel Ag_2O/Ag_2CO_3 Heterostructures with High Visible Light Efficiency in Photocatalytic Degradation of Pollutants. *Adv. Mater.* **2014**, *26*, 892−898.
(43) Dai, G.; Yu, J.; Liu, G. A New Approach for Photocorrosion Inhibition of Ag_2CO_3 Photocatalyst with Highly Visible-Light-Responsive Reactivity. *J. Phys. Chem. C* **2012**, *116*, 15519−15524.
(44) Perdew, J. P.; Burke, K.; Ernzerhof, M. Generalized Gradient Approximation Made Simple. *Phys. Rev. Lett.* **1996**, *77*, 3865−3868.
(45) Perdew, J. P.; Chevary, J. A.; Vosko, S. H.; Jackson, K. A.; Pederson, M. R.; Singh, D. J.; Fiolhais, C. Atoms, Molecules, Solids, and Surfaces: Applications of the Generalized Gradient Approximation for Exchange and Correlation. *Phys. Rev. B: Condens. Matter Mater. Phys.* **1992**, *46*, 6671−6687.
(46) Sun, D.; Fu, Y.; Liu, W.; Ye, L.; Wang, D.; Yang, L.; Fu, X.; Li, Z. Studies on Photocatalytic CO_2 Reduction over NH_2 -Uio-66(Zr) and its Derivatives: Towards a Better Understanding of Photocatalysis on Metal-Organic Frameworks. *Chem. - Eur. J.* **2013**, *19*, 14279−14285.
(47) Zhang, X.; Dong, H.; Sun, X.-J.; Yang, D.-D.; Sheng, J.-L.; Tang, H.-L.; Meng, X.-B.; Zhang, F.-M. Step-by-Step Improving Photocatalytic Hydrogen Evolution Activity of NH_2-UiO-66 by Constructing Heterojunction and Encapsulating Carbon Nanodots. *ACS Sustainable Chem. Eng.* **2018**, *6*, 11563−11569.
(48) Dong, H.; Chen, G.; Sun, J.; Li, C.; Yu, Y.; Chen, D. A Novel High-Efficiency Visible-Light Sensitive Ag_2CO_3 Photocatalyst With Universal Photodegradation Performances: Simple Synthesis, Reaction Mechanism and First-Principles Study. *Appl. Catal., B* **2013**, *134−135*, 46−54.
(49) Huang, W.; Liu, N.; Zhang, X.; Wu, M.; Tang, L. Metal-Organic Framework g-C_3N_4/MIL-53(Fe) Heterojunctions with Enhanced Photocatalytic Cctivity for Cr(VI) Reduction under Visible Light. *Appl. Surf. Sci.* **2017**, *425*, 107−116.
(50) Zhang, A.; Zhang, L.; Chen, X.; Zhu, Q.; Liu, Z.; Xiang, J. Photocatalytic Oxidation Removal of Hg^0 Using Ternary Ag/AgI-Ag_2CO_3 Hybrids in Wet Scrubbing Process under Fluorescent Light. *Appl. Surf. Sci.* **2017**, *392*, 1107−1116.
(51) Yang, J.; Dai, Y.; Zhu, X.; Wang, Z.; Li, Y.; Zhuang, Q.; Shi, J.; Gu, J. Metal-Organic Frameworks with Inherent Recognition Sites for

DOI: 10.1021/acsanm.8b01979
ACS Appl. Nano Mater. 2019, 2, 418−428

Selective Phosphate Sensing Through Their Coordination-Induced Fluorescence Enhancement effect. *J. Mater. Chem. A* **2015**, *3*, 7445−7452.
(52) Lin, K. Y.; Liu, Y. T.; Chen, S. Y. Adsorption of Fluoride to UiO-66-NH_2 in Water: Stability, Kinetic, Isotherm and Thermodynamic Studies. *J. Colloid Interface Sci.* **2016**, *461*, 79−87.
(53) Garibay, S. J.; Cohen, S. M. Isoreticular Synthesis and Modification of Frameworks with the UiO-66 Topology. *Chem. Commun.* **2010**, *46*, 7700−7702.
(54) Kandiah, M.; Nilsen, M. H.; Usseglio, S.; Jakobsen, S.; Olsbye, U.; Tilset, M.; Larabi, C.; Quadrelli, E. A.; Bonino, F.; Lillerud, K. P. Synthesis and Stability of Tagged UiO-66 Zr-MOFs. *Chem. Mater.* **2010**, *22*, 6632−6640.
(55) Zhang, L.; Yang, S.; Han, T.; Zhong, L.; Ma, C.; Zhou, Y.; Han, X. Improvement of Ag(I) Adsorption onto Chitosan/Triethanolamine Composite Sorbent by an Ion-Imprinted Technology. *Appl. Surf. Sci.* **2012**, *263*, 696−703.
(56) Liu, A.; Wang, C.-C.; Wang, C.-Z.; Fu, H.-F.; Peng, W.; Cao, Y.-L.; Chu, H.-Y.; Du, A.-F. Selective Adsorption Activities Toward Organic Dyes and Antibacterial Performance of Silver-Based Coordination Polymers. *J. Colloid Interface Sci.* **2018**, *512*, 730−739.
(57) Song, Y.; Zhu, J.; Xu, H.; Wang, C.; Xu, Y.; Ji, H.; Wang, K.; Zhang, Q.; Li, H. Synthesis, Characterization and Visible-Light Photocatalytic Performance of Ag_2CO_3 Modified by Graphene-Oxide. *J. Alloys Compd.* **2014**, *592*, 258−265.
(58) Liang, C.; Niu, C.-G.; Shen, M.-C.; Yang, S.-F.; Zeng, G.-M. Controllable Fabrication of a Novel Heterojunction Composite: AgBr and Ag@Ag_2O Co-Modified Ag_2CO_3 with Excellent Photocatalytic Performance Towards Refractory Pollutant Degradation. *New J. Chem.* **2018**, *42*, 3270−3281.
(59) Pan, B.; Xing, B. Adsorption Mechanisms of Organic Chemicals on Carbon Nanotubes. *Environ. Sci. Technol.* **2008**, *42*, 9005−9013.
(60) Ji, L.; Chen, W.; Zheng, S.; Xu, Z.; Zhu, D. Adsorption of Sulfonamide Antibiotics to Multiwalled Carbon Nanotubes. *Langmuir* **2009**, *25*, 11608−11613.
(61) Du, X.-D.; Wang, C.-C.; Liu, J.-G.; Zhao, X.-D.; Zhong, J.; Li, Y.-X.; Li, J.; Wang, P. Extensive and Selective Adsorption of ZIF-67 towards Organic Dyes: Performance and Mechanism. *J. Colloid Interface Sci.* **2017**, *506*, 437−441.
(62) Gu, Y.; Cheng, K.; Wu, Y.-N.; Wang, Y.; Morlay, C.; Li, F. Metal-Organic Framework-Templated Synthesis of Bifunctional N-Doped TiO_2-Carbon Nanotablets via Solid-State Thermolysis. *ACS Sustainable Chem. Eng.* **2016**, *4*, 6744−6753.
(63) Liu, X.; Du, P.; Pan, W.; Dang, C.; Qian, T.; Liu, H.; Liu, W.; Zhao, D. Immobilization of Uranium(VI) by Niobate/Titanate Nanoflakes Heterojunction through Combined Adsorption and Solar-Light-Driven Photocatalytic Reduction. *Appl. Catal., B* **2018**, *231*, 11−22.
(64) Tian, C.; Zhao, J.; Zhang, J.; Chu, S.; Dang, Z.; Lin, Z.; Xing, B. Enhanced Removal of Roxarsone by Fe_3O_4@3D Graphene Nanocomposites: Synergistic Adsorption and Mechanism. *Environ. Sci.: Nano* **2017**, *4*, 2134−2143.
(65) Khaletskaya, K.; Reboul, J.; Meilikhov, M.; Nakahama, M.; Diring, S.; Tsujimoto, M.; Isoda, S.; Kim, F.; Kamei, K.; Fischer, R. A.; Kitagawa, S.; Furukawa, S. Integration of Porous Coordination Polymers and Gold Nanorods into Core-Shell Mesoscopic Composites toward Light-Induced Molecular Release. *J. Am. Chem. Soc.* **2013**, *135*, 10998−11005.
(66) Li, Y.; Fang, L.; Jin, R.; Yang, Y.; Fang, X.; Xing, Y.; Song, S. Preparation and Enhanced Visible Light Photocatalytic Activity of Novel g-C_3N_4 Nanosheets Loaded with Ag_2CO_3 Nanoparticles. *Nanoscale* **2015**, *7*, 758−764.
(67) Kamat, P. V. Photochemistry on Nonreactive and Reactive (Semiconductor) Surfaces. *Chem. Rev.* **1993**, *93*, 267−300.
(68) Liang, S.; Zhou, J.; Zhang, X.; Tang, Y.; Fang, G.; Chen, T.; Tan, X. Hydrothermal Synthesis of Ag/β-$AgVO_3$ Nanobelts with Enhanced Performance as a Cathode Material for Lithium Batteries. *CrystEngComm* **2013**, *15*, 9869−9873.

DOI: 10.1021/acsanm.8b01979
ACS Appl. Nano Mater. 2019, 2, 418−428